



Fabrication of highly dispersed Ti/ZnO–Cr₂O₃ composite as highly efficient photocatalyst for naphthalene degradation

Shengjie Xia^a, Lianyang Zhang^a, Xiaobo Zhou^b, Mengmeng Shao^a, Guoxiang Pan^c, Zheming Ni^{a,*}

^a Department of Chemistry, College of Chemical Engineering, Zhejiang University of Technology, Hangzhou 310032, PR China

^b Toxikon Corporation, 15 Wiggins Ave Bedford, MA 01730, USA

^c Department of Materials Chemistry, School of Life Science, Huzhou Teachers college, Huzhou 313000, PR China

ARTICLE INFO

Article history:

Received 13 February 2015

Received in revised form 3 April 2015

Accepted 5 April 2015

Available online 7 April 2015

Keywords:

Layered double hydroxides

Ti/Schiff base

Photocatalysis

Degradation

Intermediates

ABSTRACT

In this paper, Ti-contained Schiff base complex was intercalated into the interlayer of the ZnCr layered double hydroxides (LDHs) to form a novel layered organic–inorganic nanoscale material. And then, the hybrid material was further calcined to make metal oxides composite contained Zn, Cr and Ti (Ti/ZnO–Cr₂O₃). This composite was used to study the performance and mechanism for naphthalene (L-acid) photodegradation under visible light. The characterization results showed that Ti/ZnO–Cr₂O₃ composite has higher specific area, more uniform pores size distribution and narrower band gap than that of original ZnCr–LDHs. Both physico-chemical property and photocatalytic performance for L-acid degradation by Ti/ZnO–Cr₂O₃ were greatly improved with the increasing of calcination temperature, due to the highly crystalline structures with appearance of spinel ingredients of Zn, Cr and Ti. In addition, the molar ratio of Ti/Cr would also influence the photocatalytic property of the materials. Ti/ZnO–Cr₂O₃ composite with Ti/Cr = 1 and calcined at 800 °C not only has narrow band gap (2.11 eV) and high surface area (227 m²), but also shows highest photocatalytic performance for L-acid degradation (90.2% within 240 min). Furthermore, the types and amounts of active radicals of photo oxidation reaction were also tested. The photocatalytic mechanism of the Ti/ZnO–Cr₂O₃ composite was also discussed. Moreover, based on the results from HPLC–MS, GC–MS, FT-IT and DFT analysis, the decomposition intermediates and reaction pathway for L-acid were investigated in detail.

© 2015 Elsevier B.V. All rights reserved.

1. Introduction

Layered double hydroxides (LDHs), a group of layered functional materials with special octahedral micro-structure, has the following major features: adjustable chemical composition of the layers, changeable the type and amount of the interlayer anions and controllable particle size and particle size distribution [1–3]. Replacing Mg and Al in the traditional MgAl–LDHs with Cu, Zn or Fe, new structures such as O–Cu–O, O–Zn–O and O–Fe–O could be generated and lead to dramatically decrease the band gap of the corresponding material [4,5]. Thus the valence electrons could be excited into the conduction state and creates electron–hole pair more easily, thereby, the photocatalytic oxidation–reduction activity of the material could be improved. Particularly, the photocatalytic performance of LDH materials would be improved a lot

when Ti and Cr elements are introduced [6]. Also, studies have shown that when LDH material was doped with organic complexes or other metal oxides with good photocatalytic activity, the surface properties could be changed and the photo activity could be even further improved [7].

Currently, the study of the LDHs material used as photocatalyst has been focused on the application of traditional Mg and Zn-containing LDHs for organic pollutant compound degradation reaction [8–10]. And photocatalytic objects were always traditional organic pollutants which were relatively easier to decomposed, such as azo dyes [11,12]. While, due to the property of high chromaticity, complex molecular structure, high chemical stability and low biodegradability, naphthol compounds were very hard to degrade [13,14]. At present, a few researchers have paid attention to the photodecomposition of naphthol compounds, but the LDHs materials used in these works were still traditional LDHs or their calcination products, based on our study, very little progress has been made on the study of Ti-containing LDHs material for naphthol degradation [15–17]. Our previous research showed that the

* Corresponding author. Tel.: +86 0571 88320373.

E-mail address: jchx@zjut.edu.cn (S. Xia).

photocatalytic performance would be improved after the intercalation of organic ligands contained Ti element into LDHs interlayer [18]. So far there is no research about the idea of designing a novel metal oxides composite based on Ti-containing organic-inorganic hybrid material and applying this new material on naphthol compound photo oxidation.

In this paper, Cr element was introduced into the layers to synthesize the ZnCr-LDHs, followed by introducing the Ti-containing Schiff-base complex into the LDH interlayer by ion exchange method. The prepared hybrid LDH material was further calcined at different temperature to obtain the final composite of metal oxides contained Zn, Cr and Ti. The photocatalytic performance for naphthol compound (such as L-acid) degradation of this material was further studied in detail. The influence of calcination temperature and molar ratio of Ti and Cr onto the structure and property of the composite, as well as the micro reaction kinetics, the reaction mechanism and intermediates for L-acid decomposition under visible light were investigated.

2. Experimental

2.1. Materials

L-acid ($C_{14}H_{14}N_3SO_3Na$, abbreviated as L-acid here, a typical naphthol compound), sodium 4-aminobenzoate and salicylaldehyde were guaranteed reagent (GR) and purchased from Aldrich. Titanium tetrachloride, diethyl ether and formic acid were analytical reagent (AR) and purchased from Aladdin Chemistry Co., Ltd. The others were all purchased from Zhejiang Xiaoshan Fine Chemical Co., Ltd. In addition, deionized water was decarbonated by boiling N_2 before employing in all synthesis process.

2.2. Preparation of samples

2.2.1. Synthesis of ZnCr- NO_3 -LDHs

A typical synthetic procedure was given below: an aqueous solution (100 ml) containing 20.0 g NaOH (0.50 mol) was added dropwise to a solution (150 ml) containing 44.6 g (0.15 mol) of $Zn(NO_3)_2 \cdot 6H_2O$ and 17.4 g $Cr(NO_3)_3 \cdot 9H_2O$ (0.05 mol) (initial Zn/Cr=3) with vigorous stirring at 25 °C until the final pH 8. Then, the resulting slurry was aged at 75 °C for 24 h, and then centrifuged and washed with deionized water until the pH decreased to 7. Finally it was dried in vacuo at 85 °C for 18 h. After being grounded, the product ZnCr- NO_3 -LDHs ($Zn_{0.74}Cr_{0.26}(OH)_2(NO_3)_{0.32} \cdot 0.41H_2O$ (abbreviated as Zn/Cr-LDHs) was obtained (the content of H, N, Zn and Cr: H=2.30%, N=3.65%, Zn=39.16% and Cr=11.01%).

2.2.2. Preparation of Ti/Schiff-base

In a 250 ml flask, 100 ml of ethanol solution containing 12.24 g (100 mmol) salicylaldehyde was added dropwise into a 80 ml ethanol solution containing 13.72 g (100 mmol) of sodium 4-aminobenzoate and 2 ml of formic acid with vigorous stirring for 30 min. Then, the reaction system was under refluxed for 3 h at 85 °C. The resultant slurry was then condensed, refrigerated, filtered, washed with ice-cold ethanol and dissolved with warm ethanol. This process was repeated three times. Finally the product was dried in vacuo at 65 °C for 6 h, giving the Schiff-base ligand ($C_{14}H_{10}NO_3Na$, 263 g/mol, abbreviated as SB, the yield = 63.7%, the content of C, H and N: C=62.43%, H=3.57%, N=5.49%).

And then, an ethanolic solution (80 ml) containing as-synthesized Schiff base ligand (1.422 g, 5.4 mmol) was added dropwise to a solution containing 0.35 ml (3.0 mmol) of $TiCl_4$ and 20 ml of ethanol with vigorous stirring under the N_2 atmosphere. Then, the produced suspension was continued stirred for 2 h at a refluxing temperature of 85 °C. The slurry was filtered, washed

thrice with ethanol and recrystallized from diethyl ether, finally it was dried in vacuo oven at 65 °C for 6 h, giving the product Ti/Schiff-base complex ($C_{14}H_{10}NO_3Na$)₂Ti, 573.9 g/mol, abbreviated as Ti/SB, yield, 80.1% (the content of C, H, N and Ti: C=58.17%, H=3.46%, N=4.85%, Ti=8.85%).

2.2.3. Synthesis of Ti/ZnO- Cr_2O_3 composites

First of all, the ion-exchange method was used to synthesize ZnCr-Ti/Schiff base-LDHs. The detailed process was given below: firstly, 100 ml of ethanol was added to 2.0 g dried Zn/Cr-LDHs (4.3 mmol of Cr) and stirred for 1 h; secondly, designated quality [0.608–3.644 g (1.1–6.4 mmol)] of Ti/Schiff-base complex (the molar ratio of Ti and Cr is from 0.25 to 1.5) was transferred into the above mentioned ethanolic suspension of LDH. The reaction system was refluxed at 85 °C for 24 h with constant stirring; finally, the product was isolated by filtration, washed with ethanol and dried overnight in vacuum at 65 °C, giving the product ZnCr-Ti/Schiff base-LDHs (the molar ratio of Ti/Cr=1:1 was chosen as sample: $Zn_{0.75}Cr_{0.25}(OH)_2((C_{14}H_{10}NO_3)_2Ti)_{0.18} \cdot 0.47H_2O$, abbreviated as ZnCr-Ti/SB-LDHs (the content of C, H, N, Zn, Cr and Ti: C=30.4%, H=3.28%, N=2.53%, Zn=24.5%, Cr=6.53%, Ti=4.33%. Detailed information for other samples was given in Supporting materials).

And then, 1.5 g samples were calcined in a muffle furnace with feedback-controlled microwave heating in flowing dry air at temperature range of 400–900 °C for 4 h, then grounded, giving the product Ti/ZnO- Cr_2O_3 composites (the content of Zn, Cr and Ti for sample with Ti/Cr=1:1 calcined at 800 °C is given below: Zn=51.9%, Cr=13.8% and Ti=9.10%; detailed information for other calcined composites was also given in supporting materials). The complete preparation pathway for the Ti/ZnO- Cr_2O_3 composites is depicted in Scheme 1.

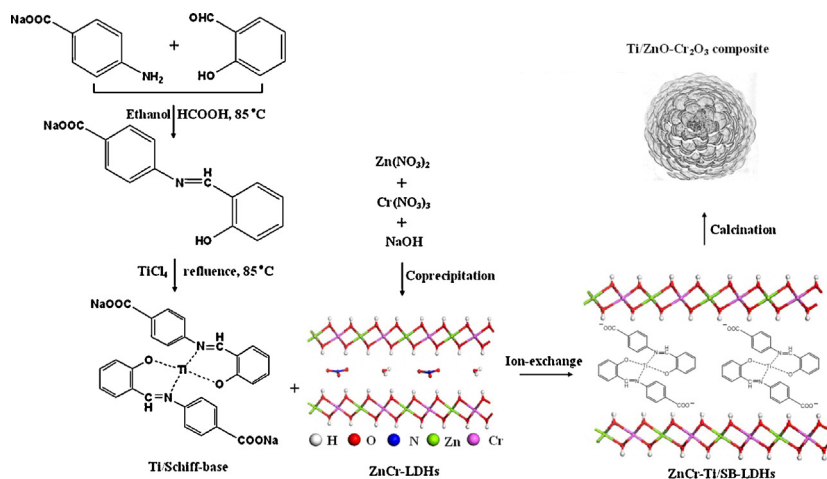
2.3. Materials characterization

Powder X-ray diffraction (XRD) patterns were recorded on a Rigaku UltimaIV powder diffractometer, using Cu K α radiation ($\lambda=1.54 \text{ \AA}$) at 40 kV and 178 mA and scanning rate of 5°/min in the range of 5–70°. SEM analysis was carried out in a Hitachi SU1510 ESEM with an acceleration voltage of 15 kV. Zn, Cr and Ti element analysis were conducted using inductively coupled plasma atomic emission spectrometry (ICP-AES) on a IRIS Intrepid II XSP instrument. Elemental microanalyses were obtained on a ThermoFinnigan Italia S.P.A elemental analyzer. The pore structure of the LDH materials was analyzed by N_2 adsorption-desorption at 77 K on a Micromeritics Instrument Corporation ASAP2020 M apparatus. Prior to the analysis, the samples were degassed in a vacuum at 120 °C for 6 h. The specific surface areas were calculated by the Brunauer-Emmett-Teller (BET) method. The pore size distribution and total pore volume were determined by the Brunauer-Joyner-Hallenda (BJH) method. Solid-state UV-vis diffuse reflectance spectra was recorded at room temperature in air by means of a Shimadzu UV-2550 spectrometer equipped with an integrating sphere attachment using $BaSO_4$ as background. Electron spin-resonance spectroscopy (ESR) was tested by a Bruker A300 EPR Spectrometer.

In addition, HPLC-MS, GC-MS and FT-IR test for photodegradation products was given in Supporting materials.

2.4. Photocatalytic reaction

The photo-catalytic activity of Ti/ZnO- Cr_2O_3 composites was monitored by degradation of L-acid under irradiation with visible light using a 500 W Xenon lamp (380 nm < λ < 760 nm, and UV light under 380 nm was filtered) equipped with a constant temperature circulator at 15 °C. Typically, a mixture of 100 ml of L-acid (50 mg/l)



Scheme 1. The complete preparation pathway for the Ti/ZnO–Cr₂O₃ composites.

solution and 100 mg of catalyst was vigorously stirred for 30 min to establish an adsorption/desorption equilibrium in dark. Then the reaction solution was stirred under visible-light irradiation for several hours under the constant temperature at 25 °C. At given time intervals, 2 ml aliquots were sampled and filtered to remove the solid phase. The filtrates was tested by measuring the absorbance at 240 nm for L-acid, by using UV–vis spectrophotometer and the blank reaction was also carried out by the same procedure without adding any catalyst.

2.5. Cluster model of LDHs and composite

According to the references [19–21], to study the structural properties of ZnCr–LDHs, the formulation of $[\text{Zn}_3\text{Cr}(\text{OH})_8]^+$ was used as the cluster model. The periodical model of $\text{Zn}_6\text{Cr}_2(\text{OH})_{16}(\text{NO}_3^-)_2$ was established in hexagonal (2H) stacking sequence, containing $\text{Zn}_3\text{Cr}(\text{OH})_8^+$ as host layer and NO_3^- as guest anion, that was the host–guest interaction model with NO_3^- in the position of hcp–Cr. And the host–guest calculation model of ZnCr–LDHs is shown in Scheme 2A. Moreover, for the purpose of reflecting the objective composition of Ti/ZnO–Cr₂O₃ composite best, we make some optimization for the calculation parameter and models. The designated molar ratios of Cr₂O₃ and TiO₂ were used to replace the adjacent ZnO (see Scheme 2B). In addition, the information of computational models for LDHs and composites was given in Supporting materials.

3. Results and discussion

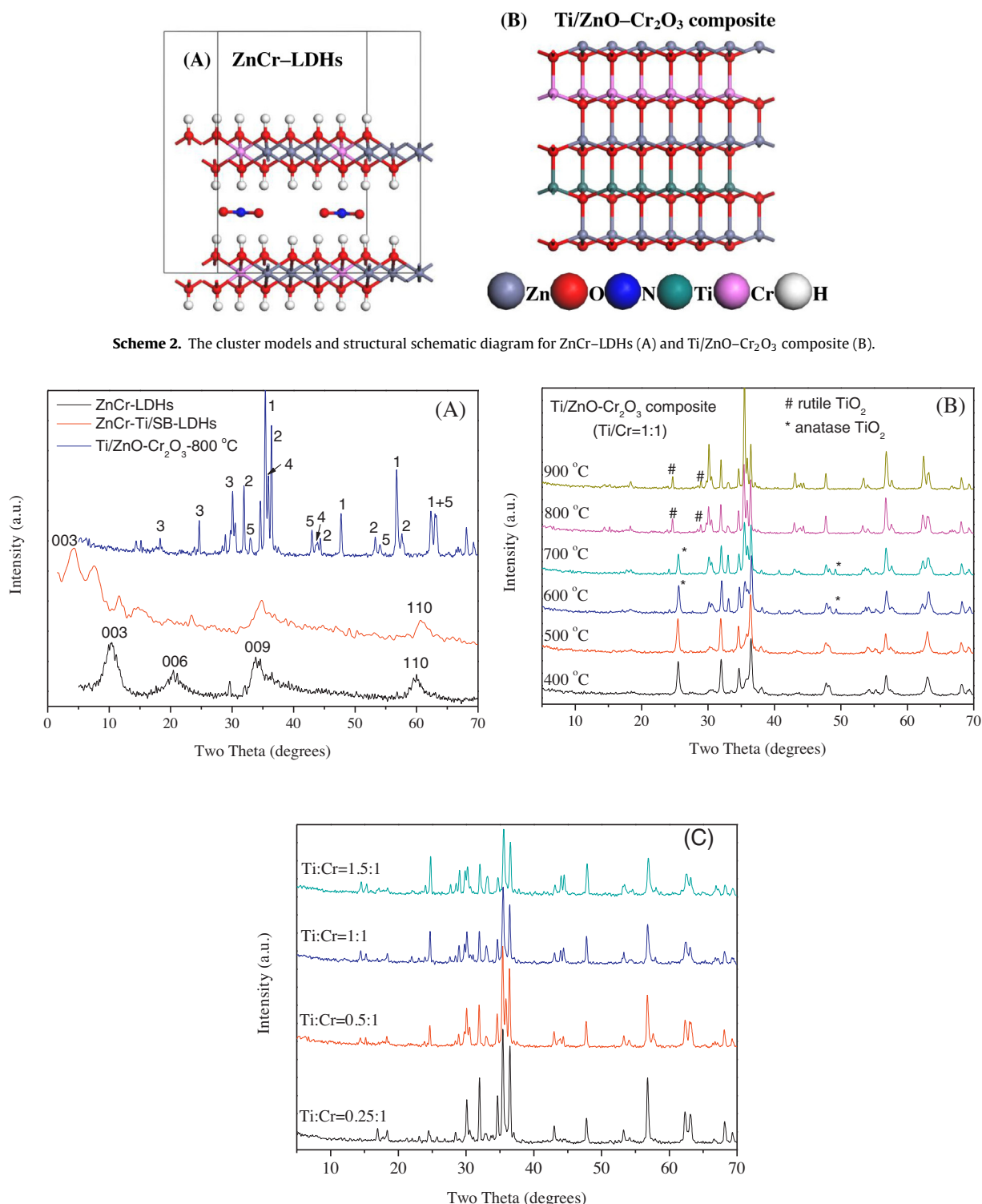
3.1. Structural characteristics of materials

Fig. 1A shows the XRD patterns of ZnCr–LDHs, ZnCr–Ti/SB–LDHs and Ti/ZnO–Cr₂O₃ composite. The expected peaks of 003, 006, 009 and 110 were observed in the sample of ZnCr–LDHs, which indicates the successful synthesis of typical LDH material. Moreover, the interlayer distance (d_{003}) of ZnCr–LDHs is 0.89 nm ($2\theta = 10.5^\circ$), which is consisted with the results reported by other authors [22,23]. For ZnCr–Ti/SB–LDHs, the typical peaks of LDHs also appear. But the interlayer distance (d_{003}) increases to 1.73 nm ($2\theta = 4.8^\circ$). The thickness of the LDH layers is 0.48 nm [24]. The gallery height of this sample after ion-exchange is 1.25 nm which can be calculated by the interlayer distance minus the thickness of the LDH layers. The increment of gallery height confirms the successful intercalation of the Ti/SB complex and formation of organic–inorganic hybrid composite. In addition, as expected, after calcination, the XRD curve of Ti/ZnO–Cr₂O₃ composite shows that

layered structure of the original LDHs was completely destroyed and indicates new peaks of metal oxides contained ZnO, Cr₂O₃, TiO₂, and spinel phase of ZnCr₂O₄ and ZnTiO₃ [10,17,25]. Particularly, compared with ZnCr–LDHs and ZnCr–Ti/SB–LDHs, the basic line of Ti/ZnO–Cr₂O₃ composite is much lower and even, the peaks were much sharper and intense, which indicates the highly crystalline structures of the latter.

The XRD patterns for Ti/ZnO–Cr₂O₃ composites calcined at 400–900 °C are given in Fig. 1B. It can be seen that there are two main differences for samples obtained by different temperatures. Firstly, as the calcination temperature increased, the crystal form of TiO₂ changed. When temperature was higher than 800 °C, most of anatase phase of TiO₂ turned to rutile phase; secondly, more and more spinel phase of ZnCr₂O₄ and ZnTiO₃ appeared with the increasing in temperature. These two structural shifts would both benefit to the improvement of Ti/ZnO–Cr₂O₃ composite [26,27]. Furthermore, Fig. 1C was the XRD patterns for Ti/ZnO–Cr₂O₃ composites with different molar ratio of Ti and Cr calcined at 800 °C. It indicated that the peaks of TiO₂ and ZnTiO₃ turned much sharper with the increasing in Ti/Cr. But the difference in XRD curves between composite with Ti/Cr = 1 and Ti/Cr = 1.5 was minute due to the limitation of ion-exchange amount of Ti/SB and nitrate ions of the ZnCr–LDHs. Namely, when ZnCr–LDHs was intercalated by Ti/SB complex with equal molar ratio of Ti and Cr, it reached the maximum of ion-exchange amount. The structure of materials with Ti/Cr = 1 and 1.5 was similar, which could be confirmed by element analysis result (see Table S1 in Supporting materials).

The SEM images of ZnCr–LDHs and Ti/ZnO–Cr₂O₃ composites are given in Fig. 2. The ZnCr–LDHs sample (Fig. 2A and B) displayed layered lamellar-shaped morphology with sharp edges which confirmed the formation of well-ordered LDH materials. Fig. 2C was the SEM image for Ti/ZnO–Cr₂O₃ composite calcined at 500 °C, which indicated the formation of irregular-shaped aggregated with grain shape. It showed that after calcination, the original layered morphology LDHs particles converted into composite of metal oxides with irregular morphology stacking particles due to the collapse of layers. Particularly, the SEM images of Ti/ZnO–Cr₂O₃ composite calcined at 800 °C (Fig. 2D and E) showed the appearance of regular flower-shaped morphology with agglomerated lamellar crystals onto the composite particles' surfaces. In addition, the result of EDS analysis (Fig. 2F) showed that main content of the composite was Zn, Cr and Ti elements. It indicated that Ti/ZnO–Cr₂O₃ composite with highly dispersed of Ti elements could be obtained from calcination of Ti/Schiff base intercalated ZnCr–LDHs at high temperature. In addition, Fig. 3 was TEM images for ZnCr–LDHs (A), Ti/ZnO–Cr₂O₃ composite calcined at 500 °C (B), Ti/ZnO–Cr₂O₃



composite calcined at 800 °C with low- (C) and high-magnification (D). As shown in Fig. 3A, ZnCr-LDHs nanoparticles displayed obvious and regular layered long flake-shaped morphology with a crystallite size of 100–200 nm. Ti/ZnO-Cr₂O₃ composite calcined at 500 °C showed irregular round plate-shape morphology with a crystallite size about 50–100 nm. It can be seen from TEM images of Fig. 3C and D, Ti/ZnO-Cr₂O₃ composite calcined at 800 °C showed a cluster constitutes with regular rectangular shape lamellar crystals.

The average diameter of those lamellar crystals was about 20–40 nm. Thus, it is obvious that Ti/ZnO-Cr₂O₃ composite calcined at 800 °C not only had smaller particle size, but also showed regular geometry of lamellar crystals than that of composite obtained from 500 °C calcination.

For further investigation of the textural parameters of Ti/ZnO-Cr₂O₃ composites, nitrogen sorption measurement was carried out. Fig. 4 shows the N₂ adsorption-desorption isotherm

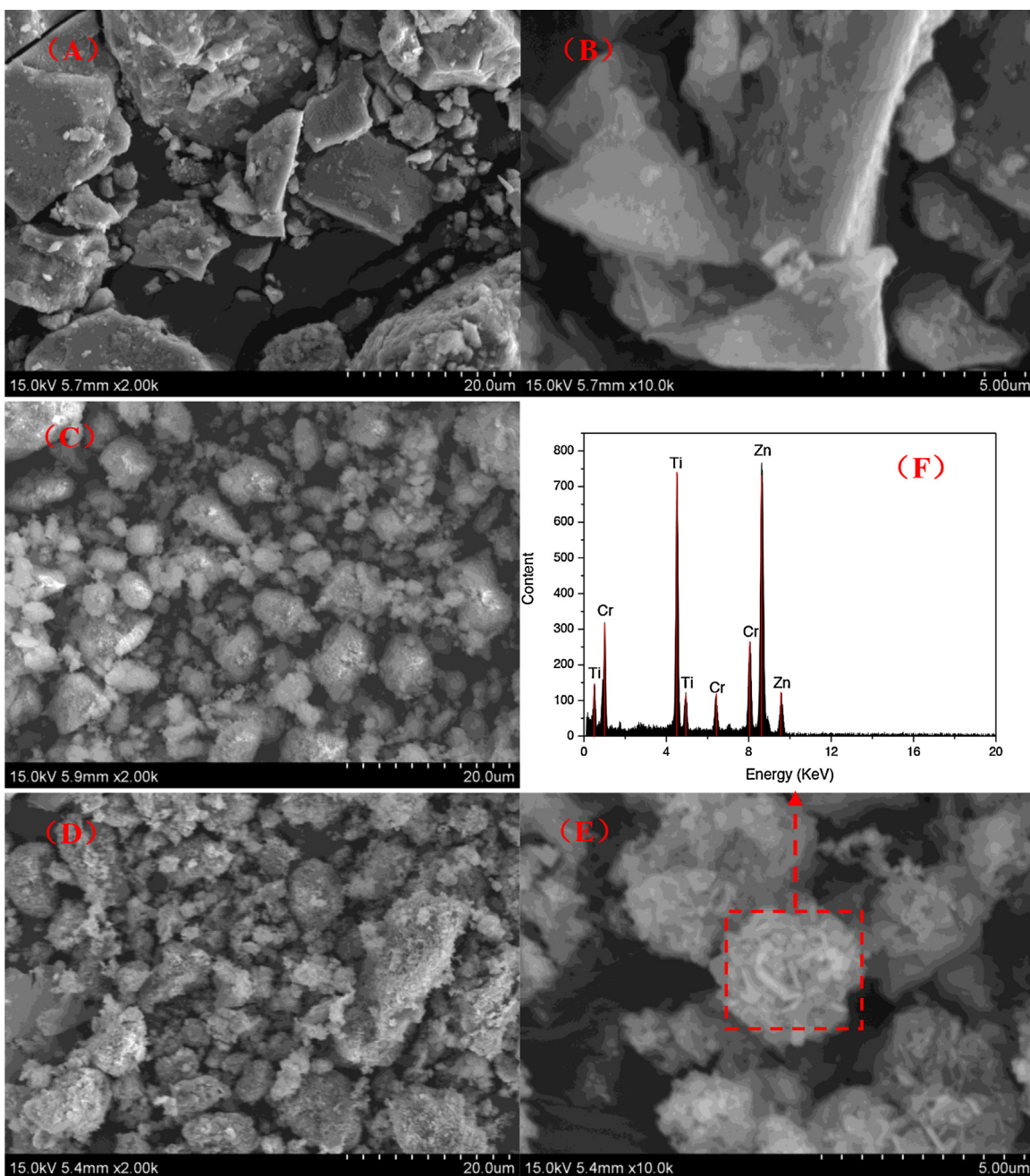


Fig. 2. SEM images for ZnCr-LDHs with low- (A) and high-magnification (B); Ti/ZnO-Cr₂O₃ composite calcined at 500 °C with low- (C); Ti/ZnO-Cr₂O₃ composite calcined at 800 °C with low- (D) and high-magnification (E); the EDS analysis of designated area (F).

at 77 K and the corresponding pore size distribution curves for ZnCr-LDHs and Ti/ZnO-Cr₂O₃ composites obtained at different conditions. The isotherms for ZnCr-LDHs (Fig. 4A) was type II with a broad H3 type hysteresis loop ($P/P_0 < 0.4$), indicating the presence of mesopores. Any limiting adsorption at higher P/P_0 was not observed, indicating the existence of macropores [28]. This result could be confirmed by the corresponding wide distribution of pore size in Fig. 4A inset. And the surface area, pore volume and pore size maximum of ZnCr-LDHs was 109 m²/g, 0.521 cm³/g and at 16 nm, 30 nm and 65 nm.

In addition, all of the isotherms for Ti/ZnO-Cr₂O₃ composites were type IV (Fig. 4B–F), which was assigned to mesoporous structure, according to the IUPAC classification. Hysteresis loops were of type H3, which were commonly attributed to slit-shaped pores generated by the aggregation of particles [29]. Particularly, although

isotherms for composites were somewhat similar, there were obvious differences in surface area, pore volume and pore size distribution. Firstly, Ti/ZnO-Cr₂O₃ composites showed larger surface area (151–234 m²/g), smaller pore volume (0.387–0.467 cm³/g) and narrower pore size distribution than that of ZnCr-LDHs. Secondly, generally speaking, with the increasing in calcination temperature and molar ratio of Ti and Cr, the surface area increased, pore size distribution became narrower, while pore volume turned smaller. But there was little variation for these parameters at calcination temperature >800 °C and Ti/Cr > 1. The surface area, pore volume and pore size maximum of Ti/ZnO-Cr₂O₃ composite (800 °C, Ti/Cr = 1) were 227 m²/g, 0.398 cm³/g and at 4.5 nm, 10 nm and 52 nm. It is obvious that the physico-chemical property of materials was greatly improved after calcination of Ti/Schiff base intercalated LDHs at high temperature.

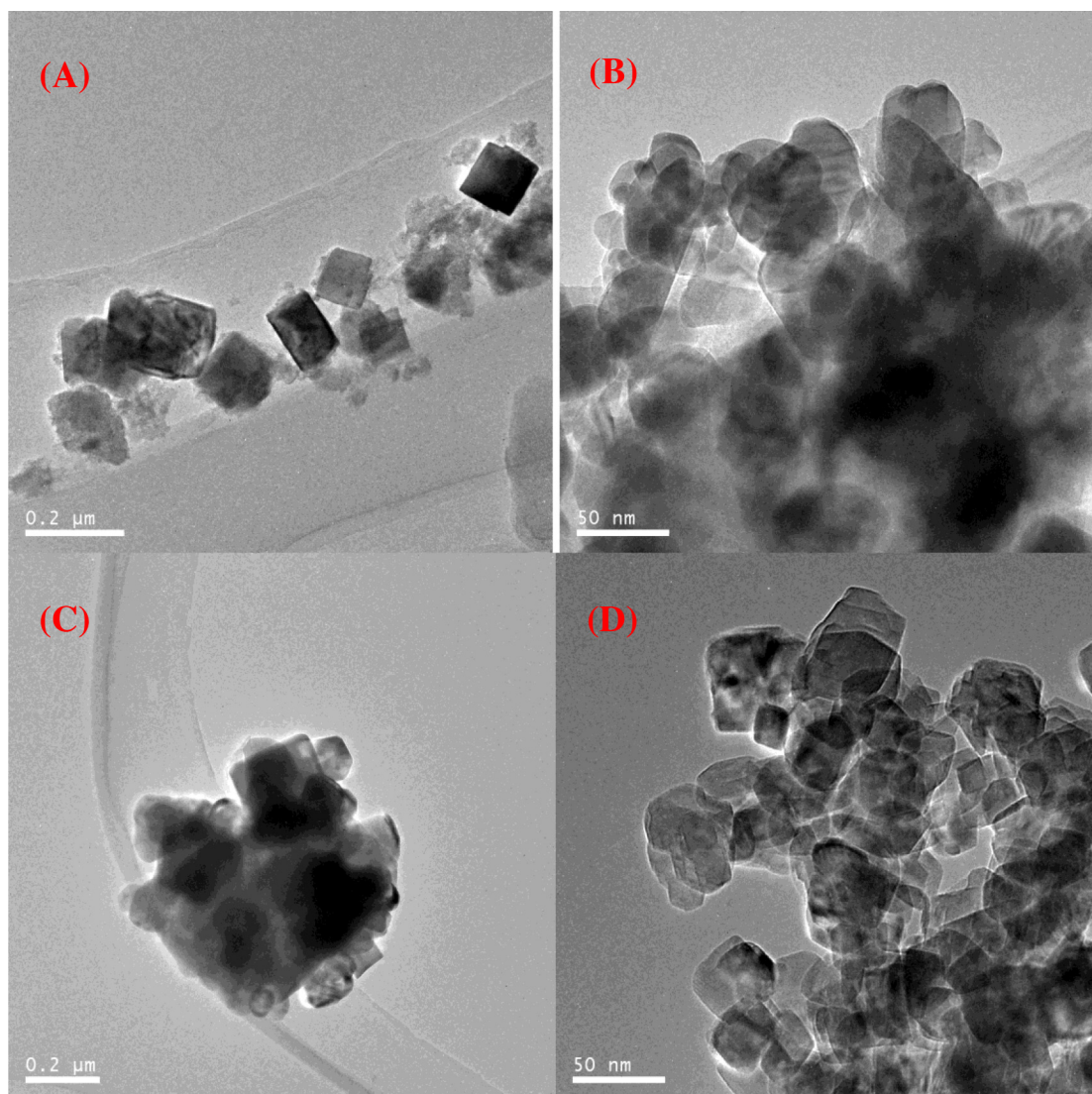


Fig. 3. TEM images for ZnCr-LDHs (A); Ti/ZnO–Cr₂O₃ composite calcined at 500 °C (B); Ti/ZnO–Cr₂O₃ composite calcined at 800 °C (Ti/Cr=1) with low- (C) and high-magnification (D).

Table 1

The band gap energy and textural properties of samples.

Catalyst	Ti/Cr	Calcined temperature(°C)	Surface area(m ² /g)	Porevolume (cm ³ /g)	Pore size distribution(nm)	E_g (eV)
ZnCr-LDHs	–	–	109	0.521	16, 30, 65	2.32
Ti/ZnO–Cr ₂ O ₃	0.25	800	178	0.459	4.8, 12, 55	2.18
Ti/ZnO–Cr ₂ O ₃	0.5	800	199	0.421	4.6, 12, 52	2.05
Ti/ZnO–Cr ₂ O ₃	1	400	151	0.475	5.0, 15, 60	2.27
Ti/ZnO–Cr ₂ O ₃	1	500	165	0.467	5.0, 15, 55	2.25
Ti/ZnO–Cr ₂ O ₃	1	600	184	0.452	5.0, 12, 55	2.21
Ti/ZnO–Cr ₂ O ₃	1	700	203	0.423	4.8, 12, 52	2.18
Ti/ZnO–Cr ₂ O ₃	1	800	227	0.398	4.5, 10, 52	2.11
Ti/ZnO–Cr ₂ O ₃	1	900	234	0.387	4.5, 12, 52	2.14
Ti/ZnO–Cr ₂ O ₃	1.5	800	231	0.390	4.5, 10, 50	2.12

The UV–vis diffuse reflectance spectra (DRS) shown in Fig. 5 were used to calculate the band gaps of ZnCr-LDHs and Ti/ZnO–Cr₂O₃ composite. The optical band gap energies of the materials were calculated using the formula $E_g = 1240/\lambda$ (nm), where λ was the wavelength corresponding to the absorption onset. The optical band gap energies of the catalysts were also shown in Table 1. The band gap of ZnCr-LDHs was about 2.32 eV, while, after intercalation and calcination, all of the Ti/ZnO–Cr₂O₃ composites showed narrower band gap than that of original LDHs.

With the increasing in the calcination temperature, the band gap of the composites showed the narrower tendency, from 2.27 to 2.11 eV for 400 to 800 °C (2.14 eV for 900 °C, which was the exception). In addition, the band gap of composite with different molar ratios was 2.18, 2.05, 2.11 and 2.12 eV for Ti/Cr=0.25, 0.5, 1 and 1.5, respectively.

To better understand the electronic band structure of both ZnCr-LDHs and Ti/ZnO–Cr₂O₃ composites, periodic density functional theory (DFT) calculation was performed to illustrate the total

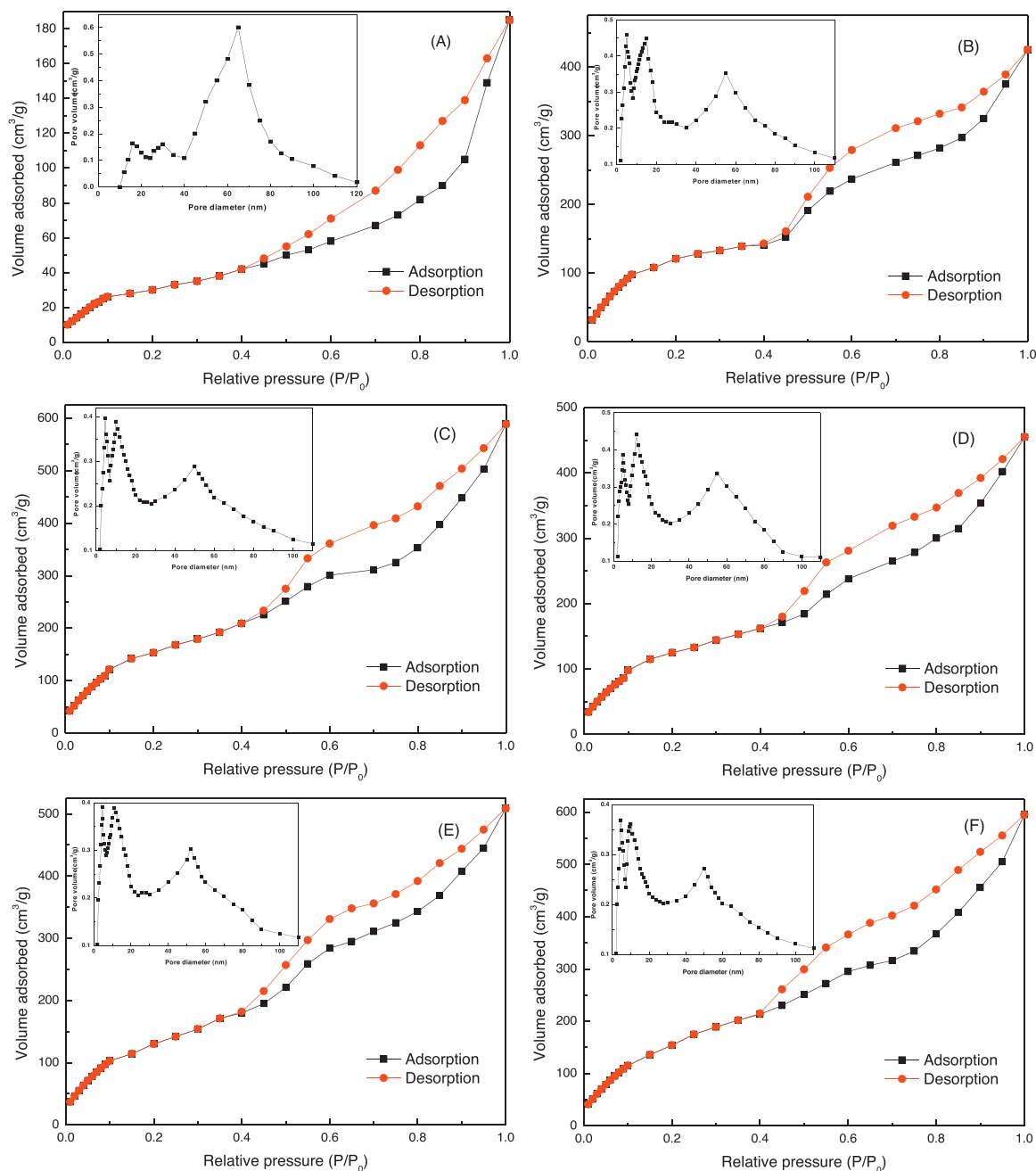


Fig. 4. N_2 sorption isotherms and pore size distribution of ZnCr-LDHs (A), Ti/ZnO–Cr₂O₃ composite at 500 and 800 °C for 1:1 (B and C); Ti/ZnO–Cr₂O₃ composite at 800 °C with Ti/Cr=0.25, 0.5 and 1.5 (D–F).

and partial electronic density of states (TDOS and PDOS) and the results were shown in Fig. 6.

The conventional DFT method always underestimates the band gap of semiconductors, especially for the composites of metal oxides [30]. For the purpose of researching the objective composition of ZnCr-LDHs and Ti/ZnO–Cr₂O₃ composite best, some optimization for the calculation parameter and models were made. Firstly, the periodical model of Zn₆Cr₂(OH)₁₆(NO₃)₂ was established in hexagonal (2H) stacking sequence, containing Zn₃Cr(OH)₈⁺ as host layer and NO₃[−] as guest anion. In addition, the designated mole ratios of Cr₂O₃ and TiO₂ were used to replace the adjacent ZnO (see Fig. 1B). The calculations were carried out by the software materials studio 5.5 with the CASTEP code. The composition of electronic band structure could be analyzed

by the density of states (DOS), and the bottoms of conduction band and the tops of valance band could be clarified [31,32]. Fig. 6 shows that the calculated band gap of ZnCr-LDHs and Ti/ZnO–Cr₂O₃ composite was 2.41 eV and 2.25 eV, respectively. For the former, the top of the VB and the bottom of the CB were mainly dominated by the 2s, 2p orbitals of O, 4s of Zn, 3d of Cr, from the LDH layers contribute to the TDOS; and for the latter, 2p of O, 4s and 3p of Zn, 3p and 3d orbitals of Cr and Ti from the metal oxides contributed a lot to the TDOS (see Fig. S2). The narrower band gap of Ti/ZnO–Cr₂O₃ composite probably resulted from the increment of Zn, Cr and Ti elements content after microwave heating of the LDH sample. These calculation results were in good agreement with the experimental results from UV–vis.

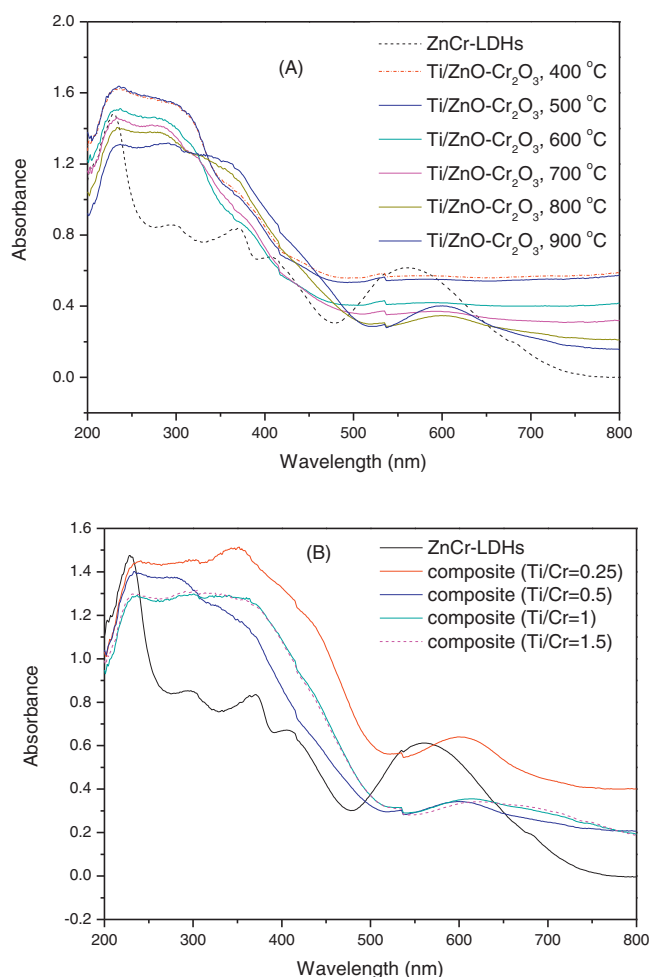


Fig. 5. The UV-vis curves for ZnCr-LDHs and Ti/ZnO-Cr₂O₃ composites: (A) indicates Ti/ZnO-Cr₂O₃ composites (Ti/Cr=1) calcined at different temperature; (B) is Ti/ZnO-Cr₂O₃ composites with different molar ratio of Ti and Cr calcined at 800 °C.

3.2. Photocatalytic properties of Ti/ZnO-Cr₂O₃ composites

To investigate the application of Ti/ZnO-Cr₂O₃ composites in photocatalysis, the photodegradation of L-acid was carried out with a reaction time ranging from 0 to 240 min, at 25 °C, pH 7.0, [L-acid] = 50 mg/L and using 100 mg of LDH materials under visible light. The results are presented in Fig. 7A and B. The result of blank experiment showed that L-acid was stable. The self-decomposition amount was only 5% after 3 h in dark. In addition, it can be seen that the photodegradation curve of L-acid by ZnCr-LDHs was relatively gentle, and the decomposition amount of L-acid by ZnCr-LDHs was only 48.7%. Nevertheless, when Ti/ZnO-Cr₂O₃ composites were used as photocatalysts, all of the degradation curves showed that the concentration of L-acid decreased rapidly in the initial 60 min and almost unchanged after 210 min (indicating reaching an equilibrium state). The decomposition amounts of L-acid catalyzed by Ti/ZnO-Cr₂O₃ increased a lot than that catalyzed by ZnCr-LDHs. Moreover, the removal rate was enhanced remarkable with the increasing of both calcination temperature and ratio of Ti and Cr, especially for Ti/ZnO-Cr₂O₃ composite obtained at 800 °C and Ti/Cr=1 (the removal rate=90.2%). Further increasing the calcination temperature and Ti/Cr resulted in little increment for removal rate. Thus, Ti/ZnO-Cr₂O₃ composites exhibited higher photocatalytic activity for L-acid degradation under visible-light irradiation,

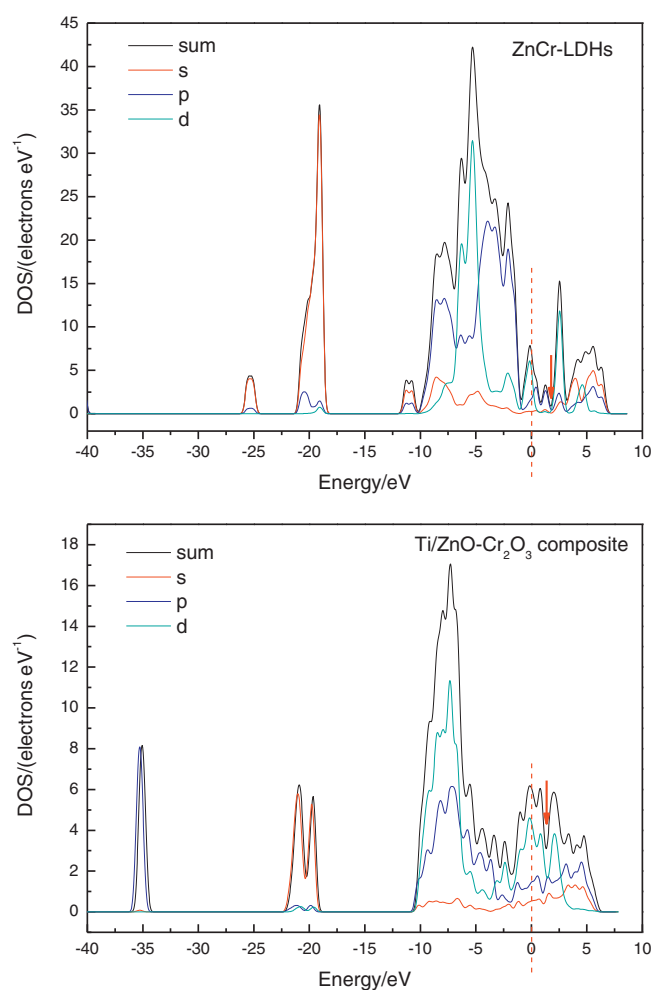


Fig. 6. Total and partial electronic density of states (TDOS and PDOS) for the ZnCr-LDHs and Ti/ZnO-Cr₂O₃ composite (Ti/Cr=1:1, 800 °C).

especially for composites prepared with Ti/Cr=1 and calcined at 800 °C.

Fig. 7C shows the photodegradation curves of total organic carbon concentration by ZnCr-LDHs and Ti/ZnO-Cr₂O₃ composite (Ti/Cr=1, 800 °C) under visible-light irradiation. The total organic carbon (TOC) removal rate was consistent with the L-acid photodegradation rate, it proves that L-acid could be decomposed by the catalyst under visible light, the naphthalene ring was opened up, also the decrease of total carbon could be caused by the formation of small molecules such as CO₂ and H₂O.

Furthermore, ZnCr-LDHs, Ti/ZnO-Cr₂O₃ composite calcined at 500 °C and 800 °C with mole ratio of Ti/Cr=1 are selected as samples to test the adsorption property for L-acid. The results are given in Fig. S3. It can be seen that the removal amount for L-acid by three samples is 10.2%, 17.4% and 22.7%, respectively, within four hours adsorption. From Fig. 7, we can see that the degradation for L-acid by three samples is 48.9%, 73.5% and 90.2%, respectively, within four hours adsorption. It means that the adsorption contributes a little for degradation of L-acid, and most of L-acid molecules are decomposed by photocatalysis.

The kinetic parameter of L-acid degradation catalyzed by ZnCr-LDHs and Ti/ZnO-Cr₂O₃ composite was investigated based on the Langmuir-Hinshelwood model, which was commonly used to describe the kinetics of photocatalytic reactions of organic compounds in aqueous solutions [33]. It relates the degradation rate r

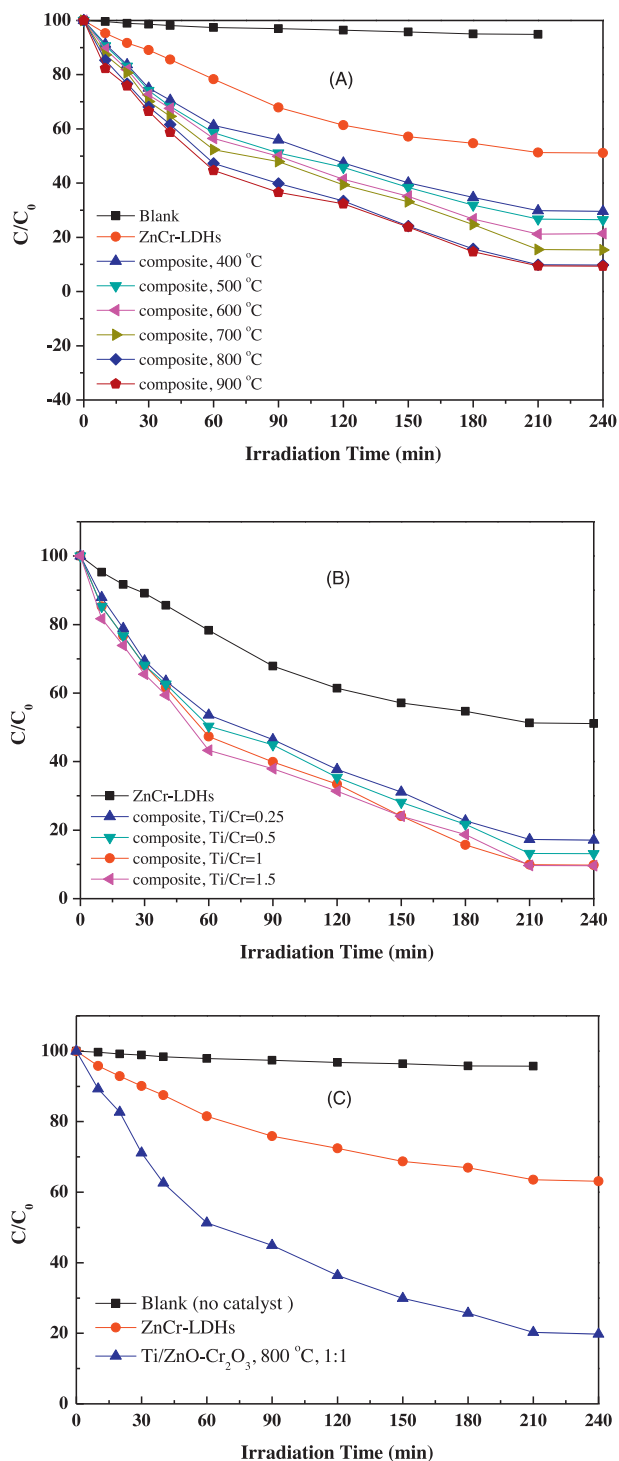


Fig. 7. The photodegradation curves of L-acid (A and B) and total organic carbon concentration (C) by samples under visible-light irradiation.

to the concentration of organic compound C, and is expressed as follows:

$$r = -\frac{dC}{dt} = \frac{k_r K_{ad} C}{1 + K_{ad} C} \quad (2)$$

where k_r is the intrinsic rate constant and K_{ad} is the adsorption equilibrium constant. When the adsorption is relatively weak and the concentration of organic compounds is low, the factor $K_{ad}C$ is

Table 2

The apparent constant, half-life and linearization coefficient for L-acid degradation by samples based on the Langmuir–Hinshelwood model.

Sample	Ti/Cr	Calced temperature(°C)	$K_{app}(\text{min}^{-1})$	$t_{1/2}(\text{min})$	r^2
ZnCr-LDHs	–	–	0.0033	210	0.9767
Ti/ZnO–Cr ₂ O ₃	0.25	800	0.0060	89	0.9861
Ti/ZnO–Cr ₂ O ₃	1	500	0.0078	115	0.9909
Ti/ZnO–Cr ₂ O ₃	1	800	0.0101	69	0.9849

insignificant, therefore the equation can be simplified to the first-order kinetics with an apparent rate constant K_{app} , as Eq. (3) shows:

$$r = k_r K_{ad} C = K_{app} C \quad (3)$$

Setting Eq. (3) under initial conditions of photocatalytic procedure, ($t=0$, $C=C_0$), Eq. (4) is obtained:

$$\ln \frac{C_0}{C} = K_{app} t \quad (4)$$

where C_0 and C are the initial concentration of L-acid and the concentration at time t , respectively. The values of apparent rate constant (K_{app}) could be calculated from the gradient of the graph of $\ln(C_0/C)$ VS irradiation time by regression method. And apparent rate constant K_{app} , L-acid half-life $t_{1/2}$ and coefficient of all the curves for ZnCr-LDHs and three typical Ti/ZnO–Cr₂O₃ composites are given in Table 2. It can be seen that linearly dependent coefficients of all the curves were all over 0.976, which showed all curves adjust well to a pseudo-first-order kinetic behavior. In addition, the rate constant was 0.0033 min^{-1} and 0.0060–0.0101 min^{-1} for ZnCr-LDHs and Ti/ZnO–Cr₂O₃ composites, respectively. It indicated that the reaction rate for L-acid photodegradation was accelerated three times after original ZnCr-LDHs processed by intercalation and calcinations. Moreover, half of L-acid photocatalyzed by the composites within a 115 min reaction, particularly, the value of $t_{1/2}$ was 69 min for Ti/ZnO–Cr₂O₃ composite with Ti/Cr = 1 calcined at 800 °C, namely, catalyzed by such composite, half of L-acid decomposed within 69 min, which was highly efficient and effective.

As a sample, Ti/ZnO–Cr₂O₃ composite (Ti/Cr = 1, 800 °C) was chosen to discuss the reutilization of those photocatalysts as efficient photocatalysts to decompose L-acid. The thermal regeneration experiments were carried out and the results were shown in Fig. S5. It showed that the progressive reduction after fourth-cycles regeneration was very small, the decomposition of L-acid was 90.2%, 89.7%, 89.2%, 88.5% and 87.3% for original composite, first-cycle, second-cycle, third-cycle and fourth-cycle, respectively. It indicated that Ti/ZnO–Cr₂O₃ composite was stable enough as photocatalyst for L-acid degradation, and the thermal regeneration for re-use of this material was feasible for at least four cycles.

3.3. Photocatalytic mechanism for L-acid degradation by Ti/ZnO–Cr₂O₃ composites

In order to investigate the reaction mechanism and degradation pathways of L-acid by Ti/ZnO–Cr₂O₃ composites, HPLC–MS, GC–MS and FT-IR test were used to analysis the complete photocatalytic process, and the detailed information was given in Supporting materials.

The naphthol ring structure has the functional groups of –SO₃H and –OH, based on the reference [34], the bonding energy of C–S and C–O are 276 kJ/mol and 364 kJ/mol, respectively, it is easier to break C–S, some researchers think the break of naphthol ring starting from the –SO₃H group for this reason. Our FT-IR results (see Fig. S6) showed the appearance of the broaden peak of SO₄^{2–} or –SO₃H at the wavelength of 1120 cm^{-1} during different reaction time, which was a solid evidence of –SO₃H oxidation

for 1-naphthol and 1,5-dihydroxynaphthalene formation. The FT-IR spectrum and new absorption peaks of L-acid degradation in different reaction time was given in Fig. S6 and Table S2 of Supporting materials. In addition, DFT calculation was used to analysis the energy structure of each atoms of L-acid, and the results are given in Table 3. According to Frontier Orbital Theory, positions with higher values of $2FED^2_{HOMO}$ are more easily subject to electron extraction, higher values of $FED^2_{HOMO} + FED^2_{LUMO}$ are more attractive for $\bullet OH$ attack [35]. As shown in Table 3, C₃ site has the highest $FED^2_{HOMO} + FED^2_{LUMO}$ value, which implied a higher possibility of mono-hydroxylation formation with $\bullet OH$ attack occurring at benzene ring. Our prediction of the possible sites for hydroxyl addition based on FEDs calculation was in well agreement with the above mentioned FT-IR result.

From the HPLC–MS and GC–MS curves for L-acid degradation in different reaction time (see Figs. S7–S9), it indicated that the main intermediates are 1-naphthol, 1,4-naphthoquinone, 5-hydroxy-1,4-naphthoquinone and (E)-vinyl but-2-enoate. Combined with the above FT-IR analysis, Table S3 summarized all the intermediates for L-acid photodegradation by Ti/ZnO–Cr₂O₃ composite.

Based on the energy band theory, when metal oxides absorbs photons with energy higher than its band gap, the excited electrons of material are promoted from the valence band to the conduction band yielding holes (h^+) and photon generated electrons (e^-). The electrons and holes react with the O₂ and H₂O absorbed at the surface of metal oxides to produce highly active radicals such as hydroxide radicals ($\bullet OH$), superoxide radicals ($\bullet O_2^-$) and peroxide free radicals ($\bullet OOH$). Essentially the photo-catalytic degradation of organic compounds is a radical reaction. The intermediate radicals could oxidize all different organic compounds directly into small molecules such as CO₂ and H₂O.

And then, to determine the radicals and explain the catalytic reaction mechanism during the photo catalytic degradation of naphthols, ESR technique was used to characterize the reaction with ZnCr–LDHs and Ti/ZnO–Cr₂O₃ composite. The results are shown in Fig. 8. There was no radical for ZnCr–LDHs under dark condition, while, it showed overlapping peaks for sextet of DMPO- $\bullet O_2^-$ and triplet of DMPO- $\bullet OOH$ after visible light irradiation. Similarly, Ti/ZnO–Cr₂O₃ composite also had no radical signal during ESR test without light exposure, while, it showed typical peaks of DMPO- $\bullet OH$ and overlapping peaks for DMPO- $\bullet O_2^-$ and DMPO- $\bullet OOH$ when

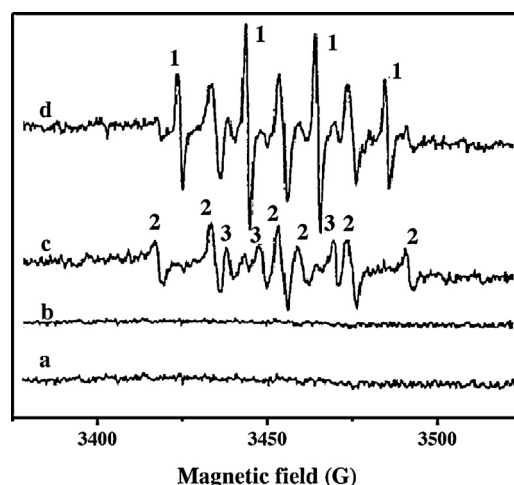


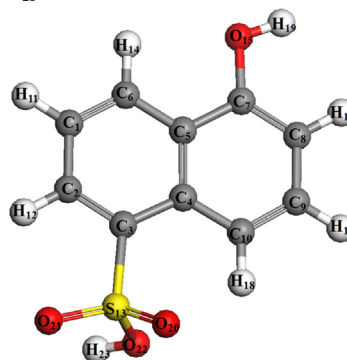
Fig. 8. ESR spectrum of ZnCr-LDHs (curve a for dark, c for visible light irradiation), and Ti/ZnO–Cr₂O₃ composite (curve b for dark, d for visible light irradiation).

material was exposed under visible light. The peaks of hydroxide radicals were more intense than that of superoxide radicals and peroxide free radicals. These results show that the oxidation reaction was gone through the traditional hydroxyl radicals as well as superoxide and peroxide free radicals, and hydroxyl radicals may are the main active radicals for photodegradation.

Furthermore, in order to investigating the influence of hydroxyl radicals into the photocatalytic property of L-acid by ZnCr-LDHs and Ti/ZnO–Cr₂O₃ composite, isopropanol (2.0 g/L) was used as a trapping agent for hydroxyl radicals ($CH_3 CH OH CH_3 + \bullet OH \rightarrow CH_3 C^{\bullet} (OH) CH_3 + H_2O$). The L-acid photodegradation contrast between inhibitor and no inhibitor are shown in Fig. 9A. It can be seen that the L-acid removal amount decreased from 90.2% to 51.5% for Ti/ZnO–Cr₂O₃ calcined at 800 °C, from 73.5% to 40.1% for Ti/ZnO–Cr₂O₃ calcined at 500 °C, from 48.9% to 30.6% for ZnCr-LDHs, when isopropanol was added. It is obviously that the concentration of hydroxyl radicals would greatly influenced the photocatalytic property of three photocatalysts. Thus, the amount of hydroxide radicals produced by photocatalytic systems was further determined using salicylaldehyde spectrophotometry [36].

Table 3
Frontier electron densities on atoms of L-acid calculated by DFT analysis.

Atom(number)	$2FED^2_{HOMO}$	$2FED^2_{HOMO} + 2FED^2_{LUMO}$	atom(number)	$2FED^2_{HOMO}$	$2FED^2_{HOMO} + 2FED^2_{LUMO}$
C ₁	0.1334	0.1540	H ₁₇	0.0001	0.0001
C ₂	0.0344	0.1999	H ₁₈	0.0003	0.0004
C ₃	0.1577	0.3545	H ₁₉	0.0003	0.0002
C ₄	0.0083	0.0326	O ₂₀	0.0136	0.0354
C ₅	0.0574	0.0371	O ₂₁	0.0077	0.0191
C ₆	0.1142	0.2950	O ₂₂	0.0135	0.0414
C ₇	0.2879	0.2845	H ₂₃	0.0001	0.0002
C ₈	0.2453	0.1561			
C ₉	0.1179	0.1529			
C ₁₀	0.4138	0.2942			
H ₁₁	0.0001	0.0001			
H ₁₂	0.0000	0.0001			
S ₁₃	0.0055	0.0532			
H ₁₄	0.0001	0.0003			
O ₁₅	0.3610	0.2134			
H ₁₆	0.0001	0.0001			



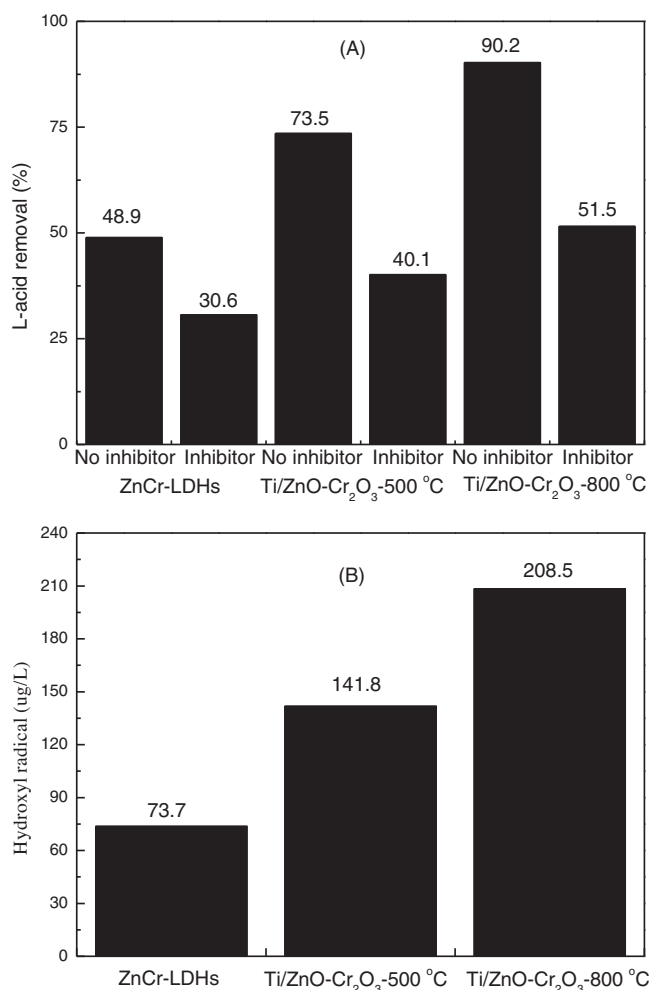


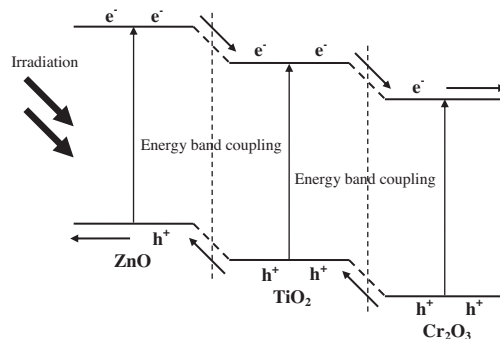
Fig. 9. The L-acid photodegradation contrast between inhibitor and no inhibitor (A) and the production of hydroxyl radical for different samples (B) (salicylaldehyde = 2 mmol/l, $t = 30$ min).

The result showed that the Ti/ZnO-Cr₂O₃ composite derived from organic-inorganic hybrid material (especially for Ti/ZnO-Cr₂O₃ calcined at 800 °C) would produce much more hydroxide radicals than ZnCr-LDHs (see Fig. 9B).

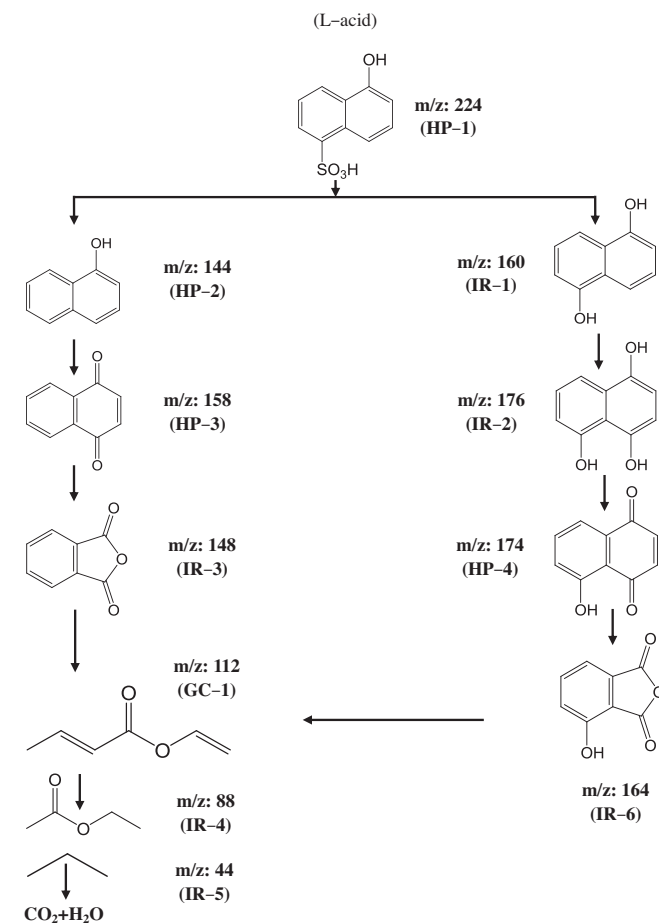
Thus, photocatalytic mechanism of the Ti/ZnO-Cr₂O₃ composites was concluded as follows: one side, materials with lower band gap has higher availability of lights, that is to say, the Ti/ZnO-Cr₂O₃ composite with lower band gap would produce more active radicals ($\cdot\text{OH}$, $\cdot\text{O}_2^-$ and $\cdot\text{OOH}$) under the same intense irradiation than that of ZnCr-LDHs. Thus, the former material shows higher photocatalytic property for degradation of organic pollutants than the latter. On the other hand, how to prevent the quick recombination of electron-hole pairs is very important for photocatalysts. Many studies have been proved that it would be an energy band coupling effect on the phase interface during the combination of different semiconductor materials. In that condition, electron-hole pairs produced from surface of the semiconductors would migrate along the vector orientation. This migration is very benefit for the photocatalytic property of the materials due to the effective inhabitation of the quick recombination of electron-hole pairs. ZnO-based semiconductor composites which have been reported contain ZnO/In₂O₃ [37], ZnO/SnO₂ [38], ZnO/NiO [39], ZnO/TiO₂ [40], ZnO/CdS [41], ZnO/ZnS [42], and so on. Thus, we speculate that it would be a similar energy band coupling effect on the phase interfaces during the combination of ZnO/Cr₂O₃/TiO₂. Under the visible light irradiation, electron-hole pairs produced from surface

of the metal oxides would migrate along the vector orientation. The migration would effectively inhabit the quick recombination of electron-hole pairs (see Scheme 3). Meanwhile, this energy band coupling effect would be strengthened with the increasing of mole ratio of Ti/Cr (Ti content), thus, composites with more Ti content show higher photocatalytic property for L-acid degradation.

Moreover, it was observed that the photocatalytic activity for L-acid degradation by Ti/ZnO-Cr₂O₃ composite enhanced with the increasing of calcined temperature. This phenomenon should be resulted from the better physicochemical property of Ti/ZnO-Cr₂O₃ composite calcined at higher temperature, such as highly crystalline structures, larger surface area and more uniform pores size distribution. These reasons were all benefit for the



Scheme 3. Schematic diagram of the energy band levels of Ti/ZnO-Cr₂O₃ composite and the transfer procedure of photogenerated e^- and h^+ pairs.



Scheme 4. The possible photocatalytic degradation pathways for L-acid by Ti/ZnO-Cr₂O₃ composite.

improvement of photocatalytic performance for L-acid decomposition by composite. Highly crystalline structures of the material not only could facilitate the rapid transfer of photoelectrons from bulk to the surface, but also effectively inhibited the recombination between photoelectrons and holes [43]. The high specific surface area was responsible for providing strong adsorption ability toward the target molecules and thus the generation of photoinduced electron–hole pairs of active sites were enhanced [44,45]. The uniform distribution of mesopores and macropores of materials was favorable for the transportation and diffusion of species.

In general, the information summary from FT-IR (Fig. S5), HPLC (Fig. S6), GC (Fig. S7) and MS (Fig. S8) analysis showed that L-acid was degraded into small molecules such as CO₂ and H₂O by going through naquinone and hydroxynaquinone intermediates under the effect of radicals ($\bullet\text{OH}$, $\bullet\text{O}_2$ —and $\bullet\text{OOH}$). The degradation process details are shown in Scheme 4.

4. Conclusions

LDHs contained Zn and Cr was synthesized by coprecipitation. It was then intercalated by Ti/Schiff base complex to form novel Ti-contained layered organic–inorganic material. This hybrid material was further calcined in a muffle furnace with feedback-controlled microwave heating to prepare the composite of metal oxides (Ti/ZnO–Cr₂O₃). The obtained Ti/ZnO–Cr₂O₃ composite showed highly dispersed Ti elements and highly crystalline structure. In addition, the electronic band structure of ZnCr–LDHs and Ti/ZnO–Cr₂O₃ composite were analyzed by periodic density functional theory (DFT) calculation, which is in good agreement with the experimental result from UV–vis. Furthermore, Ti/ZnO–Cr₂O₃ composite showed much higher photocatalytic activity than the original ZnCr–LDHs for L-acid degradation, due to the advantages of narrower band gap, special crystalline structures, larger surface area and more uniform pore size distribution. The highest values of decomposition efficiency for L-acid by the composite (Ti/Cr = 1, calcinations temperature = 800 °C) was 90.1% after 210 min of reaction. The degradation kinetics can be successfully fitted to pseudo-first-order kinetic model and Ti/ZnO–Cr₂O₃ composites are stable and could be reused at least four times. In addition, based on the results from HPLC–MS, GC–MS, FT–IT and DFT analysis, the decomposition intermediates for L-acid were naquinone and hydroxynaquinone. The oxidation reaction was gone through hydroxide radicals as well as superoxide and peroxide free radicals. Thus, this research work was designed to contribute to the photo reaction mechanism of naphthalene degradation, also dedicated to the research of other environmental contaminant removal.

Acknowledgment

This work is supported by Zhejiang Provincial Natural Science Foundation of China (LQ15B030002).

Appendix A. Supplementary data

Supplementary data associated with this article can be found, in the online version, at <http://dx.doi.org/10.1016/j.apcatb.2015.04.008>.

References

- [1] M.Q. Zhao, Q. Zhang, J.Q. Huang, F. Wei, *Adv. Funct. Mater.* 22 (2012) 675–694.
- [2] T. Nakato, H. Ueda, S. Hashimoto, R. Terao, M. Kameyama, E. Mouri, *ACS Appl. Mater. Inter.* 4 (2012) 4338–4347.
- [3] J.S. Valente, F. Tzompantzi, J. Prince, *Appl. Catal. B* 102 (2011) 276–285.
- [4] Z.J. Huang, P.X. Wu, Y.H. Lu, X.R. Wang, N.W. Zhu, Z. Dang, *J. Hazard. Mater.* 246–247 (2013) 70–78.
- [5] D. Carriazo, M. del Arco, E. Garcia-Lopez, G. Marci, C. Martin, L. Palmisano, V. Rives, *J. Mol. Catal. A-Chem.* 342–43 (2011) 83–90.
- [6] G.X. Chen, S.M. Qian, X.M. Tu, X.Y. Wei, J.P. Zou, L.H. Leng, S.L. Luo, *Appl. Surf. Sci.* 293 (2014) 345–351.
- [7] Y.F. Zhao, P.Y. Chen, B.S. Zhang, D.S. Su, S.T. Zhang, L. Tian, J. Lu, Z.X. Li, X.Z. Cao, B.Y. Wang, M. Wei, D.G. Evans, X. Duan, *Chem. Eur. J.* 18 (2012) 11949–11958.
- [8] C. Alanis, R. Natividad, C. Barrera-Diaz, V. Martinez-Miranda, J. Prince, J.S. Valente, *Appl. Catal. B* 140 (2013) 546–551.
- [9] Z.J. Huang, P.X. Wu, B.N. Gong, Y.H. Lu, N.W. Zhu, Z.X. Hu, *Appl. Surf. Sci.* 286 (2013) 371–378.
- [10] Y.Z. Wang, S.H. Luo, Z.G. Wang, Y. Fu, *Appl. Clay Sci.* 80–81 (2013) 334–339.
- [11] X.R. Wang, P.X. Wu, Y.H. Lu, Z.J. Huang, N.W. Zhu, C. Lin, Z. Dang, *Sep. Purif. Technol.* 132 (2014) 195–205.
- [12] K.M. Parida, L. Mohapatra, *Chem. Eng. J.* 179 (2012) 131–139.
- [13] X. Xiao, C.C. Xu, Y.M. Wu, P.J. Cai, W.W. Li, D.L. Du, H.Q. Yu, *Biores. Technol.* 110 (2012) 86–90.
- [14] S.X. Weng, Z.X. Pei, Z.Y. Zheng, J. Hu, P. Liu, *ACS Appl. Mater. Inter.* 5 (2013) 12380–12386.
- [15] L. Gu, F.Y. Song, N.W. Zhu, *Appl. Catal. B* 110 (2011) 186–194.
- [16] V.R. Choudhary, D.K. Dumbre, P.N. Yadav, S.K. Bhargava, *Catal. Commun.* 29 (2012) 132–136.
- [17] A. Iwaszuk, M. Nolan, Q.L. Jin, M. Fujishima, H. Tada, *J. Phys. Chem. C* 117 (2013) 2709–2718.
- [18] S.J. Xia, F.X. Liu, Z.M. Ni, W. Shi, J.L. Xue, P.P. Qian, *Appl. Catal. B* 144 (2014) 570–579.
- [19] Z.M. Ni, J. Liu, J.L. Xue, Y. Li, W. Shi, *Acta. Phys. Chim. Sin.* 28 (2012) 1714–1720.
- [20] H. Yan, J. Lu, M. Wei, J. Ma, H. Li, J. He, D.G. Evans, X. Duan, *J. Mol. Struct. Theochem.* 866 (2008) 34–45.
- [21] H. Yan, M. Wei, J. Ma, F. Li, D.G. Evans, X. Duan, *J. Phys. Chem. A* 113 (2009) 6133–6141.
- [22] N. Baliarsingh, K.M. Parida, G.C. Pradhan, *Ind. Eng. Chem. Res.* 53 (2014) 3834–3841.
- [23] M. Lan, G.L. Fan, L. Yang, F. Li, *Ind. Eng. Chem. Res.* 53 (2014) 12943–12952.
- [24] Q. Wang, D. O'Hare, *Chem. Rev.* 112 (2012) 4124–4155.
- [25] A. Venugopal, R. Sarkari, C. Anjaneyulu, V. Krishna, M.K. Kumar, N. Narender, A.H. Padmasri, *Appl. Catal. A-Gen.* 469 (2014) 398–409.
- [26] S.V. Prasanna, P.V. Kamath, C. Shivakumara, *Mater. Res. Bull.* 42 (2007) 1028–1039.
- [27] B. Leedahl, D.A. Zatselin, D.W. Boukhvalov, E.Z. Kurmaev, R.J. Green, I.S. Zhidkov, S.S. Kim, L. Cui, N.V. Gavrilov, S.O. Cholakh, A. Moewes, *J. Phys. Chem. C* 118 (2014) 28143–28151.
- [28] J. Yu, S. Liu, H. Yu, *J. Catal.* 249 (2007) 59–66.
- [29] F. Al-Wadaani, E.F. Kozhevnikova, I.V. Kozhevnikov, *J. Catal.* 257 (2008) 199–205.
- [30] J. Tang, Z. Zou, J. Ye, *J. Phys. Chem. C* 111 (2007) 12779–12785.
- [31] H. Yu, H. Irie, K. Hashimoto, *J. Am. Chem. Soc.* 132 (2010) 6898–6899.
- [32] J. Sato, H. Kobayashi, Y. Inoue, *J. Phys. Chem. B* 107 (2003) 7970–7975.
- [33] H. Fu, C. Pan, W. Yao, Y. Zhu, *J. Phys. Chem. B* 109 (2005) 22432–22439.
- [34] S. Song, H.P. Ying, Z.Q. He, J.M. Chen, *Chemosphere* 66 (2007) 1782–1788.
- [35] T. An, H. Yang, G.Y. Li, W.H. Song, J.C. William, X.P. Nie, *Appl. Catal. B* 94 (2009) 288–294.
- [36] H. Li, X.H. Li, D.J. Peng, H.L. Zheng, *Spectrosc. Spect. Anal. (China)* 27 (2007) 1591–1595.
- [37] J.S. Jang, C.J. Yu, S.H. Choi, S.M. Ji, E.S. Kim, J.S. Lee, *J. Catal.* 254 (2008) 144–155.
- [38] Z.Y. Wang, B.B. Huang, Y. Dai, X.Y. Qin, X.Y. Zhang, P. Wang, H.X. Liu, J.X. Yu, *J. Phys. Chem. C* 113 (2009) 4612–4617.
- [39] L.R. Zheng, Y.H. Zheng, C.Q. Chen, Y.Y. Zhan, X.Y. Lin, Q. Zheng, K.M. Wei, J.F. Zhu, *Inorg. Chem.* 48 (2009) 1819–1825.
- [40] L.W. Zhang, H.B. Fu, Y.F. Zhu, *Adv. Funct. Mater.* 18 (2008) 2180–2189.
- [41] M. Agrawal, S. Gupta, A. Pich, N.E. Zafeiropoulos, M. Stamm, *Chem. Mater.* 21 (2009) 5343–5348.
- [42] Y.J. Tak, H.Y. Kim, D.W. Lee, K.J. Yong, *Chem. Commun.* 38 (2008) 4585–4587.
- [43] S.Y. Chae, M.K. Park, S.K. Lee, T.Y. Kim, S.K. Kim, W.I. Lee, *Chem. Mater.* 15 (2003) 3326–3331.
- [44] M.A. Carreon, S.Y. Choi, M. Mamak, N. Chopra, G.A. Ozin, *J. Mater. Chem.* 17 (2007) 82–89.
- [45] M.Y. Wang, J. Iocozia, L. Sun, C.J. Lin, Z.Q. Lin, *Energy Environ. Sci.* 7 (2014) 2182–2202.